Developing Force Fields for Accurate Mg^{2+} and Triphosphate Interactions in ATP·Mg^{2+} Complexes

Fangchen Hu[†], Yuwei Zhang[‡], Pengfei Li[┤], Ruibo Wu[⊥] and Fei Xia*[,†]

[†]*School of Chemistry and Molecular Engineering, NYU-ECNU Center for Computational Chemistry at NYU Shanghai, East China Normal University, Shanghai 200062, China*

[‡]*Jiangsu Key Laboratory of New Power Batteries, Jiangsu Collaborative Innovation Centre of Biomedical Functional Materials, School of Chemistry and Materials Science, Nanjing Normal University, Nanjing 210023, P. R. China.*

[┤]*Department of Chemistry and Biochemistry, Loyola University Chicago, 1068 W. Sheridan Rd., Chicago, Illinois 60660, United States*

[⊥]*School of Pharmaceutical Sciences, Sun Yat-sen University, Guangzhou 510006, China*

Abstract

In cells, adenosine triphosphate(ATP) and guanosine triphosphate(GTP) molecules typically form tri-coordinated or bi-coordinated ATP·Mg^{2+} or GTP·Mg^{2+} complexes with Mg^{2+} ions and bind to proteins, participating in and regulating many important cellular functions. The accuracy of their force field parameters plays a crucial role in studying the function-related conformations of ATP·Mg^{2+} or GTP·Mg^{2+} using molecular dynamics (MD) simulations. The parameters developed based on the methyl triphosphate model in existing AMBER force fields cannot accurately describe the conformational distribution of tri-coordinated or bi-coordinated ATP·Mg^{2+} or GTP·Mg^{2+} complexes in solution. In this study, we develop force field parameters for the triphosphate group based on the new ribosyl triphosphate model, considering dihedral coupling effect, accurate van der Waals (vdW) interactions, and the influence of strongly polarized charges on conformational balance. The new parameters can accurately describe the conformational balance of tri-coordinated and bi-coordinated ATP·Mg^{2+} or GTP·Mg^{2+} conformations in solution and can be applied to simulate protein kinase.

1. INTRODUCTION

Nucleotide polyphosphate molecules such as ATP (adenosine triphosphate) and GTP (guanosine triphosphate) participate in various vital biochemical reactions within cells, playing crucial roles in the life process. Both molecules share a common structural feature, consisting of a nucleoside linked to a triphosphate group, as illustrated in **Figure 1**. When they form complexes with proteins in cells, they typically coordinate with metal cations,[1, 2] such as Mg^{2+} or Ca^{2+}. The α-, β-, and γ-O atoms in the triphosphate moiety of ATP and GTP can adopt either a tridentate (C3) or bidentate (C2) coordination conformations with Mg^{2+}. Early nuclear magnetic resonance (NMR) and spectroscopic studies[3, 4] on the conformations of ATP·Mg^{2+} in solution revealed the existence of both C3 and C2 coordination forms. These two conformations could interconvert in solution, with the C2 conformation predominating. The conformation distribution measured in experiments suggested a minimal free energy difference ΔG_{C23}(ΔG_{C2} - ΔG_{C3}) between the C2 and C3 conformations.

In order to facilitate simulation studies related to the biological functions of ATP and GTP molecules, several research groups have made significant contributions to the development of force fields for polyphosphate molecules.[5-9] Weiner et al.[5] and Pavelites et al.[7] systematically developed the force fields for polyphosphates, enabling the simulation of complex systems such as nucleotides. Meagher et al.[10] developed polyphosphate force fields for simulating ATP molecules by fitting potential energy surfaces of dihedral angles calculated from quantum mechanics calculations, based on the methyl triphosphate (MTP) model. Recently, Buelens et al.[11] employed ATP force field parameters to simulate the conformational transition between C3 and C2 states of the ATP·Mg^{2+} complex. Comparisons of the potential of mean force (PMF) profiles derived from the AMBER[10] and CHARMM22[7] force fields revealed a substantial free energy difference between the C2 conformations predicted by the two force fields, roughly exceeding 12 kcal/mol.

The free energy difference ΔG_{C23} for the ATP·Mg^{2+} complex obtained from AMBER force field simulations is roughly 7.8 kcal/mol (**Figure S1** of **Supporting Information** (**SI**)), which underestimates the stability of the C2 conformation. The

energy barrier between the calculated C3 conformation and transition state(TS) is as high as 17.0 kcal/mol. In contrast, the ΔG_{C23} result from CHARMM22 force field simulations by Branduardit et al.[12] is approximately -5.0 kcal/mol, overestimating the stability of the C2 conformation, with the energy barrier between the C3 conformation and TS around 8.7 kcal/mol. Additionally, they had also obtained a ΔG_{C23} value of approximately -2.4 kcal/mol using the CHARMM27 force fields, with an energy barrier between the C3 and TS structures of about 13.8 kcal/mol. Further, Komuro et al.[13] corrected the parameters of the P-OS-P angles of phosphate groups in the CHARMM27 force field using high-level MP2 calculations, and the corrected parameters accurately described the P-OS-P bond angle distribution of ATP in crystal structures.

As mentioned above, the phosphate group in the current AMBER force field[10] cannot accurately describe the distribution of the C3 and C2 conformations of ATP·Mg^{2+} complexes in solution and overestimates the energy barrier for conformational changes. It is thought that the reasons for these errors may include the following points: Firstly, the original force field parameters were developed from the MTP model,[10] which failed to accurately reflect the influence of the ribosyl ring on the conformation of the phosphate group. Thus, we consider to develop a new model including the ribosyl ring. Secondly, the dihedral angle parameters of the phosphate group in the original force field were only fitted to one-dimensional(1D) potential energy curves, without considering the dihedral coupling effect. Recently, Tian et al. have utilized the grid-energy correction map (CMAP)[14, 15] to parametrize backbone dihedral angles in the AMBER19SB[16] force fields, significantly enhancing the accuracy of dihedral descriptions. Thus, the CMAP will be also used to describe the dihedral interactions in the triphosphate group of the new model. Finally, the non-bonded interaction parameters derived from the early ABMER94/99[6, 17] force field describing the interaction between Mg^{2+} ions and triphosphate oxygen atoms may not accurately describe their interactions. In this work, we will refine the vdW parameters of Mg^{2+} ions and phosphate oxygen atoms using the energy decomposition analysis based on accurate density functional theory (DFT) calculations.[18, 19]

Considering these reasons, we develop new parameters for the phosphate group of ATP in the AMBER force field and explore the relevant energetic factors on conformational distribution. The new AMBER force field parameters can accurately describe the distribution of both C3 and C2 conformations of ATP·Mg^{2+} complexes in solution and can be used for simulating biomolecules not only involving ATP[20, 21], but also including GTP.[22-24]

2. Methods and Simulation Details

2.1 Potential Energy Surface Scans

The original MTP model[10] was extended to include a ribosyl ring, capped it with a hydrogen atom, resulting in the ribosyl triphosphate (RTP) model, as shown in **Figure 1**. We used the quantum mechanics (QM) package Gaussian 16[25] and employed the HF[26] and MP2[27] methods combined with the 6-31+G* basis set to recalculate potential energy curves for the six dihedral angles of the MTP model, as listed in **Table 1**. The potential energy surfaces (PES) were calculated based on the optimized MTP structure by rotating the dihedral angles in 10-degree increments. The PES scans with the HF and MP2 methods resulted in 37 data points for the MTP model (**Figure S2** of **SI**). For the larger RTP model, the atom type of the O5′ atom was changed from the original OS to a new type OY, resulting in eight specific types of the dihedral angles, as shown in **Table 1**. We used the same HF/6-31+G* level to perform PES scans at 15-degree intervals for the six dihedral angles of the RTP model.

The calculated QM energy E_l^{QM} of the *l*-th dihedral angle in the RTP model was fitted to the corresponding molecular mechanics (MM) energy E_l^{MM} using the Amber built-in program *paramfit*[28] according to eq.(1):

$$\chi_1^2 = \sum_{l=1}^{N} \omega_l \left[\left(E_l^{QM} - E_l^{MM} \right)^2 + K \right] \qquad (1)$$

In eq.(1), the residual χ_1^2 is defined to minimize the squared difference of the E_l^{MM} and E_l^{QM} energies using a genetic algorithm. The constant *K* compensates for the variations between the QM and MM energies, and the parameter ω_l is a scaling factor set to 1.0. The energy terms in the E_l^{MM} are presented in eq.(2):

$$E_l^{MM} = \sum_{Bonds} K_b(b - b_0)^2 + \sum_{Angles} K_b(b - b_0)^2 + \sum_{Dihedrals} \frac{V_n}{2}(1 + \cos(n\theta - \delta)) + \sum_{Nonbonded} \left(\frac{A_{ij}}{r_{ij}^{12}} - \frac{B_{ij}}{r_{ij}^{6}} + \frac{q_i q_j}{r_{ij}}\right) \quad (2)$$

The first and second terms denote harmonic bond and angle interactions. K_b and K_θ represent the force constants, as well as b_0 and θ_0 represent the equilibrium values of bonds and angles, respectively. The cosine functions in the third term describe dihedral angle interactions, where the parameters V_n, n, and δ represent the energy barriers, the periodicity, and the phase of dihedral angles, respectively.

When considering the dihedral coupling effect, a two-dimensional (2D) grid-energy correction map (2D-CMAP)[14, 15] can be used to improve the description for dihedral interactions in simulations. A 2D-CMAP was calculated using the HF/6-31+G* method by scanning two adjacent dihedrals at 15-degree intervals, yielding 576 data points in total. The CMAP grid in AMBER is represented using a bicubic spline function, as shown in eq.(3):

$$U_{cmap}(\varphi, \psi) = \sum_{i=0}^{3} \sum_{j=0}^{3} a_{ij} \varphi^i \psi^j \quad (3)$$

In eq.(3), a_{ij} are coefficients, and both φ and ψ are dihedral values in radians. The more details about the 2D-CMAP have been presented in previous references.[16] It is supported in the pmemd.cuda in AMEBER18.[29]

The fourth term comprises the vdW and electrostatic interactions. A_{ij} and B_{ij} represent the vdW parameters of pairwise atoms i and j in a 12-6 Lennard-Jones potential, while q_i and q_j denote the atomistic charges of atoms i and j for electrostatic interaction.

2.2 Deviation of vdW Parameters and RESP Charges

To develop accurate vdW parameters A_{ij} and B_{ij} in eq.(2) for Mg^{2+}-O coordination interactions, we adopted an approach similar to that utilized in the development of the AMOEBA+ force field.[30] The idea is to parameterize nonbonded vdW interactions

using the exchange-repulsion and dispersion-like energies calculated from high-level density functional theory (DFT) methods. It is noted that the dispersion interaction, as defined in the widely used energy decomposition analysis (EDA) based on the symmetry-adapted perturbation theory (SAPT) method,[18, 19] includes the entire Coulomb correlation and dispersion correction energies.

We used a distinct EDA scheme called the sobEDA method[31] for energy decomposition. In the sobEDA method, the sum of the exchange energy ΔE_x and the repulsion energy ΔE_{rep} is defined as the exchange-repulsion interaction ΔE_{xrep}. The sum of the DFT correction energy E_{DFTc} and the dispersion correlation ΔE_{dc} is defined as the dispersion-like Coulomb correlation ΔE_{dc}. Lu et al.[31] suggested that the sum of the E_{xrep} and ΔE_{dc} energies in the sobEDA method appropriately corresponds to the exchange-repulsion correlation and dispersion correction energies in the SAPT method when using the accurate B3LYP-D3(BJ) functional.[32-34] Therefore, the summed energies of the ΔE_{xrep} and ΔE_{displ} were employed to derive the vdW parameters between the Mg^{2+} ion and the other atoms in the ATP.

To reduce computational cost, we initially utilized a simplified RTP·Mg^{2+} model instead of the whole ATP·Mg^{2+} to perform umbrella sampling (US)[35] simulations for the conformational change from the C3 to C2 structures. Subsequently, a total of 216 conformations were randomly extracted from the different windows of the US simulation, including C3, C2, and transition state (TS) structures. Next, 216 single-point energy calculations were conducted on these structures using the accurate B3LYP-D3(BJ)/6-31+G** method. The sobEDA method[31] was employed for energy decomposition to obtain the ΔE_{xrep} and ΔE_{displ} energies from single-point calculations. Finally, a least-square fitting was carried out by using the gradient descent method to minimize the residual χ_2^2 defined in eq.(5):

$$\chi_2^2 = \sum_{m=1}^{M=216} \left(E_m^{QM,vdW} - \sum_{n=1}^{N=30} E_{m,n}^{MM,vdW} \right)^2 \qquad (5)$$

In eq.(5), the first term $E_m^{QM,vdW}$ refers to the QM energy summations of the ΔE_{xrep} and ΔE_{displ} that are calculated from the m-th structure among the M = 216

conformations. The second term $E_{m,n}^{MM,vdW}$ denotes the calculated vdW interaction MM energies between the Mg^{2+} ion and the other $N = 30$ atoms of the RTP model in the m-th structure. The physical meaning of minimizing χ_2^2 is to yield the optimal vdW parameters A_{ij} and B_{ij} indicated in eq.(2) for Mg^{2+} and ATP.

The original atomic charges of ATP used in the AMBER force fields are based on the RESP[17] charges calculated at the HF/6-31+G* method. It is known that the RESP charges calculated from HF method in vaccum tend to overestimate molecular dipoles, indirectly accounting for solvent effects. Alternatively, we propose using the B3LYP-D3(BJ)/6-311+G** method combined the PCM model with a dielectric constant 78.35 to calculate the RESP charges of ATP. Atomic charges are determined using the standard RESP procedure.

2.3 MD Simulation Details and Umbrella Sampling

The C3 conformation of the ATP·Mg^{2+} complex was extracted from the crystal structure 1B38[36] and served as the initial structure in our simulations. The ATP·Mg^{2+} complex was immersed in a TIP3P[37] water box with a length of 14 Å and neutralized with two Na^+ ions. The ATP parameters developed by Meagher et al.[10] and the compromise Mg^{2+} parameters developed by Li et al.[38] were used for the ATP·Mg^{2+} complex. The SHAKE[39] algorithm was employed to maintain constraints on H-containing bonds. A nonbonded cutoff of 10 Å was used, and long-range electrostatic interactions were treated using the Particle Mesh Ewald[40] method. The whole system underwent energy minimization, followed by heating in the NVT ensemble. The temperature was maintained at 300 K using a Langevin thermostat[41] with a collision frequency of 2.0 ps^{-1}, and the pressure was maintained at 1.0 bar using the Berendsen barostat.[42] The equilibration of the system was carried out in the NPT ensemble at 300 K with an integration step of 2 fs, utilizing the Amber ff14SB[43] force fields within the AMBER18 package.[29]

In the US simulation, the distance of the Mg^{2+} ion and the O_α atom, denoted as Mg^{2+}-O_α, is chosen as the 1D reaction coordinate. The range of the Mg^{2+}-O_α distance spans from 1.7 to 5.9 Å, in line with that chosen in the previous simulations.[11] The range

of 1.7-5.9 Å was divided into 43 windows with a 0.1 Å interval. In each window, a 5 ns US simulation was conducted using a harmonic potential added on the Mg^{2+}-Oα distance, with a force constant of 150 kcal·mol^{-1}·Å^{-2}. Next, the US trajectories were used to plot 1D PMF curves using the WHAM method.[44]

2.4 Replica-Exchange MD (REMD) Simulations and Analysis

A total of 22 replicas spanning a temperature range of 300–420 K were employed for 150 ns REMD simulations.[45] The temperature for each replica was generated using a tool available at https://jerkwin.github.io/gmxtools. The REMD simulations were initiated from the C3 structures of the ATP·Mg^{2+} complex. We used the pypdb library to collect 169 ATP·Mg^{2+} complexes in the crystal structures of proteins from the PDB database, focusing on the C2 and C3 conformations. Principal component analysis (PCA) was performed on the backbones of triphosphate groups in ATP and the Mg^{2+} ions using the CPPTRAJ[46] module in the AMBER package. The first two components, PC1 and PC2, from the PCA were used as coordinates to construct two-dimensional free energy landscapes (2D-FELs). The crystal structures of the 169 ATP·Mg^{2+} complexes and the REMD trajectories were projected onto the 2D-FELs to yield the distributions of the C3 and C2 structures using the WHAM method.[44]

3. Results and Discussion

3.1 The Ribosyl Triphosphate (RTP) Model

We first employed HF/6-31+G* to recalculate the 1D potential energy curves of the six dihedral angles calculated by Meagher et al.[10] previously. The calculated black curves (**Figure S2** of **SI**) match completely with their published results. To validate the influence of high-level methods on the calculation of dihedral angle potential energy curves, we utilized the MP2/6-31+G* method to perform more accurate energy calculations based on HF-optimized structures. The resulting black curves in **Figure S2** of **SI** shows no significant difference from that of HF/6-31+G*. This indicates that merely using high-level method cannot effectively improve the computational results. Therefore, we attempt to develop a new model for parameterizing the triphosphate group in GTP/ATP.

As shown in **Figure 1**, the triphosphate groups in real ATP or GTP molecules are connected to the ribose rings. However, a hydrogen atom was used instead of ribose in the MTP model to cap the C5' atom, which failed to reflect the steric influence of ribose on the changes in dihedral angles with the triphosphate group. In this work, we propose the ribosyl triphosphate (RTP) model instead of the MTP model to parameterize the triphosphate group. The advantage of the RTP model lies in including the ribose moiety, thus being able to reflect the impact of ribose on the conformations of triphosphate group. Considering the more atoms in the RTP model than the MTP model and the insignificant difference in the PES curves calculated by HF and MP2, we still chose to utilize the HF/6-31+G* method to conduct PES calculations on the crucial dihedral angles in the RTP model.

Figure 2a-2f display the results of restrained PES scans for dihedral angles in the RTP model. In **Figure 2a** and **2b**, it is observed that the curves for the dihedrals O1G-PG-O3B-PB and PG-O3B-PB-O3A show little difference compared to those from the MTP model. However, the energy curves for the dihedral angles O3B-PB-O3A-PA, PB-O3A-PA-O5′, O3A-PA-O5′-C5′, and PA-O5′-C5′-C4′ in **Figures 2c-2f** exhibit marked differences, especially in **Figures 2e** and **2f**, where discrepancies with the MTP model are particularly pronounced. For instance, the two minima of the MTP curve in **Figure 2e** are located at approximately 70 ° and 310 °, with identical energies. In contrast, the RTP model has two unequal minima, and yields a result at 310 ° that is approximately 15.0 kcal/mol higher than the MTP. In **Figure 1f**, the PA-O5′-C5′-C4′ dihedral angle in the MTP model exhibits three energy minima due to the periodicity of the arbitrary CH_3 group, located at 60 °, 180 °, and 300 ° respectively. By contrast, the RTP model presents two unequal minima at 90 ° and 225 °. This discrepancy is obviously caused by the presence of the ribose moiety in the RTP model, which introduces a strong steric effect on the rotation of the PA-O5′-C5′-C4′ dihedral angle, thus eliminating the pseudo-periodicity of the CH_3 group observed in the MTP model.

3.2 Dihedral Parameters for the RTP Model

Based on the torsion energy curves in **Figure 2**, we employed the *paramfit* program to derive the fitted parameters for the P-OS-P angle and dihedral angles according to eq.(1) (**Figure S3** of **SI**). **Table 1** presents the new parameters derived for the dihedrals and the P-OS-P angle of the RTP model. The original parameters of the MTP model are also included in **Table 1** for comparison. The original MTP model possesses six types of dihedral angles, namely, P-OS-P-O3, P-OS-P-O2, P-OS-P-OS, CT-OS-P-O2, CT-OS-P-OS, and HC-CT-OS-P. In the MTP model of **Figure 1**, all the three atoms O5′, O3A, and O3B atoms belong to the atom type OS. Considering the heterogeneous environment of the O5′ atom is different from the that of O3A and O3B atoms, we designated a new atom type OY instead of OS for the O5′ atom in the RTP model. Thus, the original P-OS-P-OS dihedral type in the MTP model split into two types of dihedrals, namely, P-OS-P-OS and P-OS-P-OY. The specific dihedral PB-O3A-PA-O5′ is now described with the new dihedral interaction P-OS-P-OY rather than the original P-OS-P-OS. Similarly, the original dihedral types CT-OS-P-O2, CT-OS-P-OS, and HC-CT-OS-P are renamed into CT-OY-P-O2, CT-OY-P-OS, and HC-CT-OY-P, respectively. As a result, the RTP model has seven dihedral angles and an angle type P-OS-P in total.

Comparing the derived dihedral parameters of both models, we find that they differ significantly from each other due to the large difference in **Figure 2**. The value of the equilibrium angle P-OS-P obtained from our fitting is 142.9°, close to the 150.0° from the MTP model.[10] In order to validate these parameters, we conducted US simulations to estimate the PMF curve for the ATP·Mg^{2+} transition from the C3 to C2 conformations. In **Figure 3a**, the black and blue curves represent the results from the MTP and RTP models, respectively. The MTP model utilized the original parameters of Meagher et al.[10], while the RTP model employed the new dihedral and angle parameters in **Table 1**. The MTP curve shows that the Mg^{2+}-O distance in the stable C2 conformation is 3.90 Å, with an energy 7.8 kcal/mol higher than the C3 conformation, consistent with the reported findings.[11] With the new parameters, the PMF curve from the RTP model suggests that the most stable C2 conformation has an Mg^{2+}-O distance of 4.81 Å, with a corresponding energy of 7.1 kcal/mol. It can be seen that the RTP

model does not exhibit a clear enhancement compared to the MTP model. The barriers of TS for the MTP and RTP models are 16.9 and 16.3 kcal/mol, respectively.

3.3 The Grid-Energy Correction Map

To accurately account for the influence of dihedral angle changes on conformations, it is necessary to consider coupled effects among dihedral interactions in MD simulation. It can be seen in **Figures 2c-2f** that the four curves of the RTP model show substantial alterations due to the presence of the ribose moiety. Thus, we focused on the coupled interactions among the following three pairs of dihedrals in the parenthesis corresponding to that in **Figure 1**, namely, (O3B-PB-O3A-PA, PB-O3A-PA-O5'), (PB-O3A-PA-O5', O3A-PA-O5'-C5'), and (O3A-PA-O5'-C5', PA-O5'-C5'-C4'). Employing the HF/6-31+G* method, we have performed 2D-PES scans for the three pairs of dihedrals, generating corresponding 2D-CMAPs. However, due to the convergence issues encountered in restricted calculations, we have only obtained the full 2D-CMAP in **Figure 3b** for the pair of the two dihedrals O3B-PB-O3A-PA and PB-O3A-PA-O5′. This 2D-CMAP provides a richer energetic insight into the interplay between the two adjacent dihedrals.

Hence, we estimated the PMF curve for the transition between C2 and C3 conformations using the 2D-CMAP in US simulations, and the outcome is displayed as the blue curve in **Figure 3a**. Compared to the red PMF without including the 2D-CMAP, the blue curve following the inclusion of the 2D-CMAP appears smoother in the range of 3.0 to 6.0 Å, demonstrating two relatively stable energy regions in the range of 4.0-5.5 Å. The free energy difference ΔG_{23} measured from the blue curve is 5.3 kcal/mol, a reduction of 2.5 kcal/mol from the 7.8 kcal/mol observed in the MTP model. The simulation results inferred that accounting for dihedral interactions via the CMAP method reduced the difference in conformational free energies, albeit only by 2.5 kcal/mol. Further considerations of other factors influencing conformational equilibria are required to achieve more accurate results.

3.4 Refinement of vdW Parameters from DFT Calculations

In the simulation study of the ATP·Mg^{2+} complex by Buelens et al.[11], the vdW parameters of Mg^{2+} ions and O atoms were sourced from the optimized parameters for Mg^{2+} by Li et al.[38] and the ones for O2 atoms in the ABMER94/99 force fields. A question about whether the used vdW parameters could accurately describe the coordination interaction remains unverified. Inspired by the method used by Liu et al.[30] in developing vdW parameters for the AMOEBA+ force field, we attempt to parameterize vdW interactions using exchange-repulsion and dispersion energies obtained from accurate DFT calculations.

To reduce computational cost, we initially utilized a simplified ATP·Mg^{2+} model, referred to as the RTP·Mg^{2+} model, for US simulations. Subsequently, 216 conformations were randomly sampled from the trajectories in different US windows, including the C3, C2, and TS structures during conformational transition. Next, single-point energy calculations were performed on these structures using the accurate B3LYP-D3(BJ)/6-31+G** method. The sobEDA method[31] was utilized for energy decomposition to obtain the exchange-repulsion energy ΔE_{xrep} and dispersion correction energy ΔE_{displ}, then yielding the summed QM energy $E^{QM,vdW}$. Finally, a least-square fitting was conducted on the QM energy $E^{QM,vdW}$ and the MM energy $E^{MM,vdW}$ according to eq.(4). The derived pairwise vdW parameters A_{ij} and B_{ij} for the interactions of Mg^{2+} ions with the O and P atoms are shown in **Table 2**. The results show that the A_{ij} values for the O3 and O2 types differ significantly between the two sets of parameters. The value of the original A_{ij} is 26767.87 kcal·Å^{12}/mol, but the DFT-derived ones is 56958.78 kcal·Å^{12}/mol. Besides, the A_{ij} and B_{ij} parameters for the OS, OY, and P atom types show no significant difference.

Figure 4a illustrates the fitting of the QM energy $E^{QM,vdW}$ with the MM energies $E^{MM,vdW}$ calculated from the original and DFT-derived vdW parameters. From the comparative results, it can be observed that the original vdW parameters severely underestimated the exchange-repulsion and dispersion interaction energies between Mg^{2+} and O atoms, especially the exchange-repulsion energy. The weaker vdW repulsion resulted in a stronger attraction between Mg^{2+} and O atoms, requiring higher

energy to break the Mg^{2+}-O_α coordination bond, thereby leading to a higher relative energy for transition to the C2 conformation. The root-mean square deviation (RMSD) between the QM energies and DFT-derived ones is only 5.06 kcal/mol, with a Pearson correlation coefficient 0.938. In contrast, the vdW energies calculated from original parameters showed a RMSD of 33.72 kcal/mol from the QM energies.

Figure 4b shows the PMF curve of conformational changes obtained using the DFT-derived vdW parameters. Compared to the 5.3 kcal/mol in **Figure 3a**, the free energy difference ΔG_{C23} between the C2 and C3 conformations decreased to 0.30 kcal/mol, with only a 0.65 kcal/mol difference from -0.35 kcal/mol implied by the crystal structure distribution.[11] The Mg^{2+}-O_α distance in the stable C2 conformation is 4.07 Å. The barrier of TS also decreased to a reasonable value of 11.1 kcal/mol compared to the 16.3 kcal/mol from the original parameters. It can be drawn a conclusion that accurately fitting force field parameters using precise DFT calculations can indeed improve the description of vdW interactions between the pairwise Mg^{2+} and O atoms.

3.5 Polarized Charges for Electrostatic Interactions

The charges calculated using the HF/6-31G* method in vacuum conditions were actually overestimated by approximately 10-15% compared to experimental values.[17] Therefore, the vacuum charges obtained by the HF method can be considered to include some polarization effects. Recently, computational studies by Zhou et al.[47] have shown that accurate DFT methods under the PCM solvent model yield molecular dipole moments larger than those calculated by the HF method in vacuum. This suggests that charges obtained using B3LYP under the PCM model include stronger polarization effects. For example, Duan et al. used B3LYP with the PCM model to compute charges in the early development of the AMBER03 force field.[48] Considering the strong polarization effect of the P atom in the phosphate group in solution, we aim to obtain a set of charges containing stronger polarization effects to describe the electrostatic interactions of the phosphate group. We recalculated the RESP charges of the phosphate

group using the B3LYP/6-311+G** method under the PCM model with a dielectric constant 78.35 based on the RTP model.

The fitted RESP charges for each atom in the RTP model are shown in **Table S1** of **SI**. Comparing the two sets of charges, we observe that the differences are primarily concentrated on the heavy atoms. We also compared the molecular dipoles calculated by the two methods, with slightly larger results obtained from B3LYP/6-311+G**. To verify the impact of these stronger polar charges on conformational changes, we combined the 2D-CMAP, the DFT-derived vdW parameters, and the DFT-derived charges to simulate the conformational changes of the ATP·Mg^{2+} complex from the C3 to C2 conformations.

3.6 Distributions of REMD Conformations and Crystal Structures

Figure 5a presents the PMF curve depicting the conformational changes of the ATP·Mg^{2+} complex simulated using the B3LYP-derived charges. The computed relative free energy ΔG_{C23} is -0.86 kcal/mol, closely matching the -0.35 kcal/mol suggested by the crystal structure distribution and aligning with NMR experimental results. The PMF curve from the simulation indicates that the Mg^{2+}-O_α distances for the stable conformations C3 and C2 are 2.06 Å and 4.06 Å, respectively. The energy barrier for the TS is 11.3 kcal/mol, which is consistent with the nearly 13.8 kcal/mol obtained from Charmm27 simulations.[12]

To further validate the effectiveness of the B3LYP-derived charges, we performed PCA analysis on the backbones of the C3 and C2 structures for the ATP·Mg^{2+} complexes and plotted a distribution map of crystal structures. The 150 ns REMD simulation trajectories of the ATP·Mg^{2+} complexes using the HF charges and B3LYP charges were then projected onto the distribution maps, as shown in **Figure 5b** and **5c,** respectively. Comparing **Figures 5b** and **5c**, it can be observed that the REMD simulation using B3LYP charges effectively samples both the C3 and C2 regions. The two sampled regions closely match the distributions of the corresponding crystal C3 and C2 structures. In contrast, the REMD simulation using the HF charges did not

effectively sample the C2 conformation, primarily because the PMF predicted an unfavorable 0.30 kcal/mol for the C2 conformation.

4. Conclusion

In this study, we developed force field parameters for the triphosphate group in ATP and GTP molecules based on the new RTP model. During the force field development process, we mainly considered several factors influencing the distribution of the C3 and C2 conformations. Firstly, we introduced ribose into the original MTP model, considering its influence on the conformation connecting the triphosphate group. We recalculated the 1D potential energy curves of dihedral angles based on the RTP model and found significant differences compared to MTP. Secondly, we introduced 2D-CMAP potential to describe the coupling effects between dihedral angles, which led to significant improvements. Next, to improve the description of the interaction between Mg^{2+} and O atoms by the original vdW parameters, we refined more accurate parameters through high-level DFT calculations and energy decomposition. Using the original HF charges, the 2D-CMAP, and the DFT-derived vdW parameters, the value of ΔG_{C23} decreased to 0.3 kcal/mol.

Additionally, we utilized the B3LYP/6-311+G** method to compute a new set of polarizable charges under the PCM model and explored the impact of strong polarization charges on the balance between C3 and C2 conformations. We found that the ΔG_{C23} calculated using strong polarization charges was -0.86 kcal/mol, which more closely matched the results implied by NMR experiments. Further REMD simulations demonstrated that the new force field parameters could effectively sample the C3 and C2 conformations of the ATP·Mg^{2+} complexes, with conformational distributions highly consistent with those indicated by crystal structures. Through the comparison of the aforementioned research results, we discovered that developing accurate vdW parameters for Mg^{2+} and O is crucial for accurately describing the conformational balance of the ATP·Mg^{2+} complexes. In future applications, we recommend using strong polarization charges derived from B3LYP, along with the calculated 2D-CMAP and DFT-derived vdW parameters, to simulate protein systems containing the

$ATP{\cdot}Mg^{2+}$ and $GTP{\cdot}Mg^{2+}$ complexes The relevant parameter files have been attached and the script for using the new parameters is shown in **Section S1** of **SI**.

ASSOCIATED CONTENT

Supporting Information

Figure S1 presents the estimated 1D-PMF of the $ATP{\cdot}Mg^{2+}$ complex using AMBER force fields. **Figure S2** presents the scanned PES curves for dihedral angles using the HF and MP2 methods. **Figure S3** presents fitted results based the RTP model. **Table S1** presents a comparison of the original HF charges and B3LYP-derived charges. **Section S1** provides a script for using the new developed parameters.

AUTHOR INFORMATION

Corresponding Authors

*Emails: fxia@chem.ecnu.edu.cn (F.X.)

ORCID

Yuwei Zhang: 0009-0002-8741-3889

Pengfei Li: 0000-0002-2572-5935

Ruibo Wu: 0000-0002-1984-046X

Fei Xia: 0000-0001-9458-9175

ACKNOWLEDGMENT

This work was supported by the National Natural Science Foundation of China (No. 22073029). P.L. acknowledges the financial support by the start-up funds from Loyola University Chicago (to P.L.). We also acknowledge the support of the NYU-ECNU Center for Computational Chemistry at NYU Shanghai as well as the ECNU Public Platform for Innovation (001) for providing computer time.

References:

1. Li, P.; Merz, K. M., Jr. Metal Ion Modeling Using Classical Mechanics. *Chem. Rev.* **2017,** *117* (3), 1564-1686.

2. Li, P.; Song, L. F.; Merz, K. M., Jr. Systematic Parameterization of Monovalent Ions Employing the Nonbonded Model. *J. Chem. Theory Comput.* **2015,** *11* (4), 1645-57.

3. Huang, S. L.; Tsai, M.-D. Does the Magnesium(II) Ion Interact with the -Phosphate of Adenosine. *Biochemistry* **1982,** *21* (5), 951-959.

4. Takeuchi, H.; Murata, H.; Harada, I. Interaction of Adenosine 5'-Triphosphate with Mg2 Vibrational Study of Coordination Sites by Use of 18Q-Labeled. *J. Am. Chem. Soc.* **1988,** *91* (5), 1629-1637.

5. Weiner, S. J.; Kollman, P. A.; Case, D. A.; Singh, U. C.; Ghio, C.; Alagona, G.; Profeta, J., S.; Weiner, P. A New Force Field for Molecular Mechanical Simulation of Nucleic Acids and Proteins. *J. Am. Chem. Soc.* **1984,** *106* (3), 765-784.

6. Cornell, W. D.; Cieplak, P.; Bayly, C. I.; Gould, I. R.; Merz, J., K. M.; Ferguson, D. M.; Spellmeyer, D. C.; Fox, T.; Caldwell, J. W.; Kollman, P. A. A Second Generation Force Field for the Simulation of Proteins, Nucleic Acids and Organic Molecules. *J. Am. Chem. Soc.* **1995,** *117* (19), 5179-5197.

7. Pavelites, J. J.; Gao, J. A Molecular Mechanics Force Field for NAD+, NADH, and the Pyrophosphate. *J. Comput. Chem.* **1997,** *18* (2), 221-239.

8. Petrova, P.; Koca, J.; Imberty, A. Potential Energy Hypersurfaces of Nucleotide Sugars: Ab Initio Calculations, Force-Field Parametrization, and Exploration of the Flexibility. *J. Am. Chem. Soc.* **1999,** *121* (23), 5535-5547.

9. Koca Findik, B.; Jafari, M.; Song, L. F.; Li, Z.; Aviyente, V.; Merz, K. M., Jr. Binding of Phosphate Species to Ca(2+) and Mg(2+) in Aqueous Solution. *J. Chem. Theory Comput.* **2024**.

10. Meagher, K. L.; Redman, L. T.; Carlson, H. A. Development of Polyphosphate Parameters for Use with the AMBER Force Field. *J. Comput. Chem.* **2003,** *24* (9), 1016–1025.

11. Buelens, F. P.; Leonov, H.; de Groot, B. L.; Grubmuller, H. ATP-Magnesium

Coordination: Protein Structure-Based Force Field Evaluation and Corrections. *J. Chem. Theory Comput.* **2021,** *17* (3), 1922-1930.

12. Branduardi, D.; Marinelli, F.; Faraldo-Gomez, J. D. Atomic-resolution dissection of the energetics and mechanism of isomerization of hydrated ATP-Mg(2+) through the SOMA string method. *J. Comput. Chem.* **2016,** *37* (6), 575-86.

13. Komuro, Y.; Re, S.; Kobayashi, C.; Muneyuki, E.; Sugita, Y. CHARMM Force-Fields with Modified Polyphosphate Parameters Allow Stable Simulation of the ATP-Bound Structure of Ca(2+)-ATPase. *J. Chem. Theory Comput.* **2014,** *10* (9), 4133-42.

14. Mackerell, A. D., Jr.; Feig, M.; Brooks, I., C. L. Extending the Treatment of Backbone Energetics in Protein Force Fields: Limitations of Gas-phase Quantum Mechanics in Reproducing Protein Conformational Distributions in Molecular Dynamics Simulations. *J. Comput. Chem.* **2004,** *25* (11), 1400-15.

15. MacKerell, J., A. D.; Feig, M.; Brooks, I., C. L. Improved Treatment of the Protein Backbone in Empirical Force Fields. *J. Am. Chem. Soc.* **2004,** *126* (3), 698-699.

16. Tian, C.; Kasavajhala, K.; Belfon, K. A. A.; Raguette, L.; Huang, H.; Migues, A. N.; Bickel, J.; Wang, Y.; Pincay, J.; Wu, Q.; Simmerling, C. ff19SB: Amino-Acid-Specific Protein Backbone Parameters Trained against Quantum Mechanics Energy Surfaces in Solution. *J. Chem. Theory Comput.* **2020,** *16* (1), 528-552.

17. Wang, J.; Cieplak, P.; Kollman, P. A. How Well Does a Restrained Electrostatic Potential (RESP) Model Perform in Calculating Conformational Energies of Organic and Biological Molecules? *J. Comput. Chem.* **2000,** *21* (12), 1049–1074.

18. Jeziorski, B.; Moszynski, R.; Szalewicz, K. Perturbation Theory Approach to Intermolecular Potential Energy Surfaces of van der Waals Complexes. *Chem. Rev.* **1994,** *94* (7), 1887-1930.

19. Stasyuk, O. A.; Sedlak, R.; Guerra, C. F.; Hobza, P. Comparison of the DFT-SAPT and Canonical EDA Schemes for the Energy Decomposition of Various Types of Noncovalent Interactions. *J. Chem. Theory Comput.* **2018,** *14* (7), 3440-3450.

20. Zhang, Y.; Cao, Z.; Zhang, J. Z.; Xia, F. Double-Well Ultra-Coarse-Grained

Model to Describe Protein Conformational Transitions. *J. Chem. Theory Comput.* **2020,** *16* (10), 6678-6689.

21. Zha, J.; Xia, F. Developing Hybrid All-Atom and Ultra-Coarse-Grained Models to Investigate Taxol-Binding and Dynein Interactions on Microtubules. *J. Chem. Theory Comput.* **2023,** *19* (16), 5621-5632.

22. Zeng, J.; Weng, J.; Zhang, Y.; Xia, F.; Cui, Q.; Xu, X. Conformational Features of Ras: Key Hydrogen-Bonding Interactions of Gln61 in the Intermediate State during GTP Hydrolysis. *J. Phys. Chem. B* **2021,** *125* (31), 8805-8813.

23. Xiong, Y.; Zeng, J.; Xia, F.; Cui, Q.; Deng, X.; Xu, X. Conformations and binding pockets of HRas and its guanine nucleotide exchange factors complexes in the guanosine triphosphate exchange process. *J. Comput. Chem.* **2022,** *43* (13), 906-916.

24. Zeng, J.; Chen, J.; Xia, F.; Cui, Q.; Deng, X.; Xu, X. Identification of functional substates of KRas during GTP hydrolysis with enhanced sampling simulations. *Phys. Chem. Chem. Phys.* **2022,** *24* (13), 7653-7665.

25. Gaussian 16, Revision C.01, Frisch, M. J.; Trucks, G. W.; Schlegel, H. B.; Scuseria, G. E.; Robb, M. A.; Cheeseman, J. R.; Scalmani, G.; Barone, V.; Petersson, G. A.; Nakatsuji, H.; Li, X.; Caricato, M.; Marenich, A. V.; Bloino, J.; Janesko, B. G.; Gomperts, R.; Mennucci, B.; Hratchian, H. P.; Ortiz, J. V.; Izmaylov, A. F.; Sonnenberg, J. L.; Williams-Young, D.; Ding, F.; Lipparini, F.; Egidi, F.; Goings, J.; Peng, B.; Petrone, A.; Henderson, T.; Ranasinghe, D.; Zakrzewski, V. G.; Gao, J.; Rega, N.; Zheng, G.; Liang, W.; Hada, M.; Ehara, M.; Toyota, K.; Fukuda, R.; Hasegawa, J.; Ishida, M.; Nakajima, T.; Honda, Y.; Kitao, O.; Nakai, H.; Vreven, T.; Throssell, K.; Montgomery, J. A., Jr.; Peralta, J. E.; Ogliaro, F.; Bearpark, M. J.; Heyd, J. J.; Brothers, E. N.; Kudin, K. N.; Staroverov, V. N.; Keith, T. A.; Kobayashi, R.; Normand, J.; Raghavachari, K.; Rendell, A. P.; Burant, J. C.; Iyengar, S. S.; Tomasi, J.; Cossi, M.; Millam, J. M.; Klene, M.; Adamo, C.; Cammi, R.; Ochterski, J. W.; Martin, R. L.; Morokuma, K.; Farkas, O.; Foresman, J. B.; Fox, D. J. Gaussian, Inc., Wallingford CT, 2016.

26. Roothaan, C. C. J. New Developments in Molecular Orbital Theory. *Rev. Mod. Phys.* **1951,** *23* (2), 69-89.

27. Frisch, M. J.; Head-Gordon, M.; Pople, J. A. A Direct MP2 Gradient Method. *Chem. Phys. Lett.* **1990,** *166* (3), 275-280.

28. Betz, R. M.; Walker, R. C. Paramfit: Automated Optimization of Force Field Parameters for Molecular Dynamics Simulations. *J. Comput. Chem.* **2015,** *36* (2), 79-87.

29. Case, D. A.; Cheatham, T. E., 3rd; Darden, T.; Gohlke, H.; Luo, R.; Merz, K. M., Jr.; Onufriev, A.; Simmerling, C.; Wang, B.; Woods, R. J. The Amber Biomolecular Simulation Programs. *J. Comput. Chem.* **2005,** *26* (16), 1668-88.

30. Liu, C.; Piquemal, J.-P.; Ren, P. AMOEBA+ Classical Potential for Modeling Molecular Interactions. *J. Chem. Theory Comput.* **2019,** *15* (7), 4122-4139.

31. Lu, T.; Chen, Q. Simple, Efficient, and Universal Energy Decomposition Analysis Method Based on Dispersion-Corrected Density Functional Theory. *J. Phys. Chem. A* **2023,** *127* (33), 7023-7035.

32. Becke, A. D. Density-functional Exchange-energy Approximation with Correct Asymptotic Behavior. *Phys. Rev. A* **1988,** *38* (6), 3098-3100.

33. Lee, C.; Yang, W.; Parr, R. G. Development of the Colle-Salvetti Correlation-energy Formula into a Functional of the Electron Density. *Phys. Rev. B* **1988,** *37* (2), 785-789.

34. Grimme, S.; Ehrlich, S.; Goerigk, L. Effect of the Damping Function in Dispersion Corrected Density Functional Theory. *J. Comput. Chem.* **2011,** *32* (7), 1456-65.

35. Torrie, G. M.; Valleau, J. P. Nonphysical Sampling Distributions in Monte Carlo Free-energy Estimation: Umbrella Sampling. *J. Comput. Phys.* **1977,** *23* (2), 187-199.

36. Brown, N. R.; Noble, M. E. M.; Lawrie, A. M.; Morris, M. C.; Tunnah, P.; Divita, G.; Johnson, L. N.; Endicott, J. A. Effects of Phosphorylation of Threonine 160 on Cyclin-dependent Kinase 2 Structure and Activity. *J. Biol. Chem.* **1999,** *274* (13), 8746–8756.

37. Jorgensen, W. L.; Chandrasekhar, J.; Madura, J. D.; Impey, R. W.; Klein, M. L. Comparison of Simple Potential Functions for Simulating Liquid Water. *J. Chem. Phys.* **1983,** *79* (2), 926-935.

38. Li, P.; Roberts, B. P.; Chakravorty, D. K.; Merz, K. M., Jr. Rational Design of Particle Mesh Ewald Compatible Lennard-Jones Parameters for +2 Metal Cations in Explicit Solvent. *J. Chem. Theory Comput.* **2013,** *9* (6), 2733-2748.

39. Ryckaert, J. P.; Ciccotti, G.; Berendsen, H. J. C. Numerical Integration of a System with Constraints: of the Cartesian Equations of Motion Molecular Dynamics of n-Alkanes. *J. Comput. Phys.* **1977,** *23* (3), 321-341.

40. Salomon-Ferrer, R.; Gotz, A. W.; Poole, D.; Le Grand, S.; Walker, R. C. Routine Microsecond Molecular Dynamics Simulations with AMBER on GPUs. 2. Explicit Solvent Particle Mesh Ewald. *J. Chem. Theory Comput.* **2013,** *9* (9), 3878-88.

41. Pastor, R. W.; Brooks, B. R.; Szabo, A. An Analysis of the Accuracy of Langevin and Molecular Dynamics Algorithms. *Mol. Phys.* **1988,** *65* (6), 1409-1419.

42. Berendsen, H. J. C.; Postma, J. P. M.; van Gunsteren, W. F.; DiNola, A.; Haak, J. R. Molecular Dynamics with Coupling to an External Bath. *J. Chem. Phys.* **1984,** *81* (8), 3684-3690.

43. Maier, J. A.; Martinez, C.; Kasavajhala, K.; Wickstrom, L.; Hauser, K. E.; Simmerling, C. ff14SB: Improving the Accuracy of Protein Side Chain and Backbone Parameters from ff99SB. *J. Chem. Theory Comput.* **2015,** *11* (8), 3696-3713.

44. Kumar, S.; Rosenberg, J. M.; Bouzida, D.; Swendsen, R. H.; Kollman, P. A. THE weighted histogram analysis method for free-energy calculations on biomolecules. I. The method. *J. Comput. Chem.* **2004,** *13* (8), 1011-1021.

45. Sugita, Y.; Okamoto, Y. Replica-exchange Molecular Dynamics Method for Protein Folding. *Chem. Phys. Lett.* **1999,** *314* (1-2), 141–151.

46. Roe, D. R.; Cheatham, T. E. PTRAJ and CPPTRAJ: Software for Processing and Analysis of Molecular Dynamics Trajectory Data. *J. Chem. Theory Comput.* **2013,** *9* (7), 3084-3095.

47. Zhou, A.; Schauperl, M.; Nerenberg, P. S. Benchmarking Electronic Structure Methods for Accurate Fixed-Charge Electrostatic Models. *J. Chem. Inf. Model.* **2020,** *60* (1), 249-258.

48. Duan, Y.; Wu, C.; Chowdhury, S.; Lee, M. C.; Xiong, G.; Zhang, W.; Yang, R.; Cieplak, P.; Luo, R.; Lee, T.; Caldwell, J.; Wang, J.; Kollman, P. A

Point-Charge Force Field for Molecular Mechanics Simulations of Proteins based on Condensed-phase Quantum Mechanical Calculations. *J. Comput. Chem.* **2003,** *24* (16), 1999-2012.

Table 1. The angle and dihedral parameters of the RTP models are derived by fitting the potential energy curves of the dihedral angles shown in **Figure 1** using the HF/6-31+G* method. For the dihedral angels, $V_n/2$ represents the magnitude of the torsions in kcal/mol, γ denotes the phase offset in degrees, and n indicates the periodicity. The K_θ and θ represent the force constant and equilibrium value of the P-O-P angle, respectively.

Models		**MTP**			**RTP**			
No.	**Dihedrals**	$V_n/2$	γ	n	**Dihedrals**	$V_n/2$	γ	n
1	P-OS-P-O3	0.085	0	3	P-OS-P-O3	0.197	-18.92	3
2	P-OS-P-O2	0.355	0	2	P-OS-P-O2	0.204	103.11	2
3	P-OS-P-OS	0.897	0	1	P-OS-P-OS	2.867	-18.72	1
					P-OS-P-OY	0.796	8.48	1
4	CT-OS-P-O2	-0.406	0	2	CT-OY-P-O2	-1.193	68.39	2
		0.590	0	3		-0.308	150.63	3
5	CT-OS-P-OS	-1.560	0	1	CT-OY-P-OS	-2.577	121.18	1
6	HC-CT-OS-P	0.035	0	3	H1-CT-OY-P	1.401	164.87	3
	Angle	K_θ	θ		**Angle**	K_θ	θ	
7	P-OS-P	12.685	150.0		P-OS-P	20.117	142.9	

Table 2 Comparison of the original and DFT-derived vdW parameters A_{ij} and B_{ij} for the pairwise interactions between the Mg^{2+} ion and P atoms as well as various types of O atoms. The units of A_{ij} and B_{ij} are kcal·Å^{12}/mol and kcal·Å^{6}/mol, respectively. For the oxygen atoms, the parameters for the atom types O3 and O2, as well as OS and OY, are identical.

Atom Types	**O3, O2**	**OS, OY**	**P**
Original A_{ij}	26767.87	26326.74	132977.70
DFT-derived A_{ij}	55958.78	26407.56	133097.78
Original B_{ij}	70.40	66.22	155.01
DFT-derived B_{ij}	69.26	66.18	154.94

Figure 1 An illustration of the structures of the tri-coordinated(C3) or bi-coordinated(C2) conformations of the ATP·Mg^{2+} or GTP·Mg^{2+} complexes. For the MTP and ATP models, the left structure displays the atomic names in AMBER force fields, while the right cartoons show the corresponding atomic types.

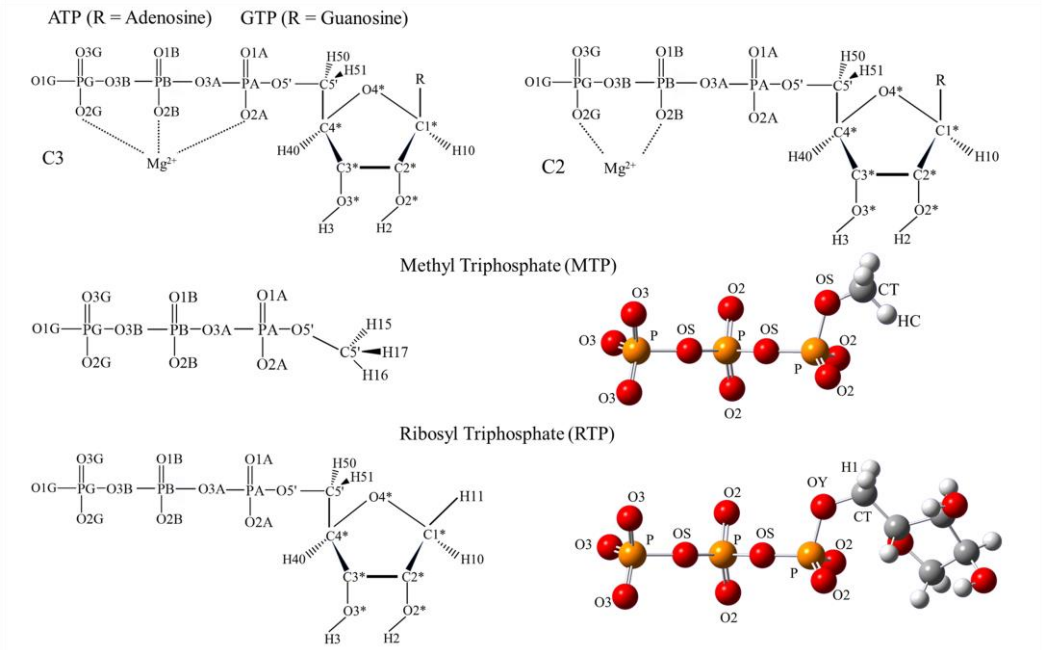

Figure 2(a)-2(f) Calculated potential energy curves for the dihedrals O1G-PG-O3B-PB, PG-O3B-PB-O3A, O3B-PB-O3A-PA, PB-O3A-PA-O5′, O3A-PA-O5′-C5′, and PA-O5′-C5′-C4′, respectively. The black and red curves denote the results of the MTP and RTP models, respectively. Dihedral angles were scanned at 15-degree intervals using the HF/6-31+G* method. The rotation energy is measured in kcal/mol.

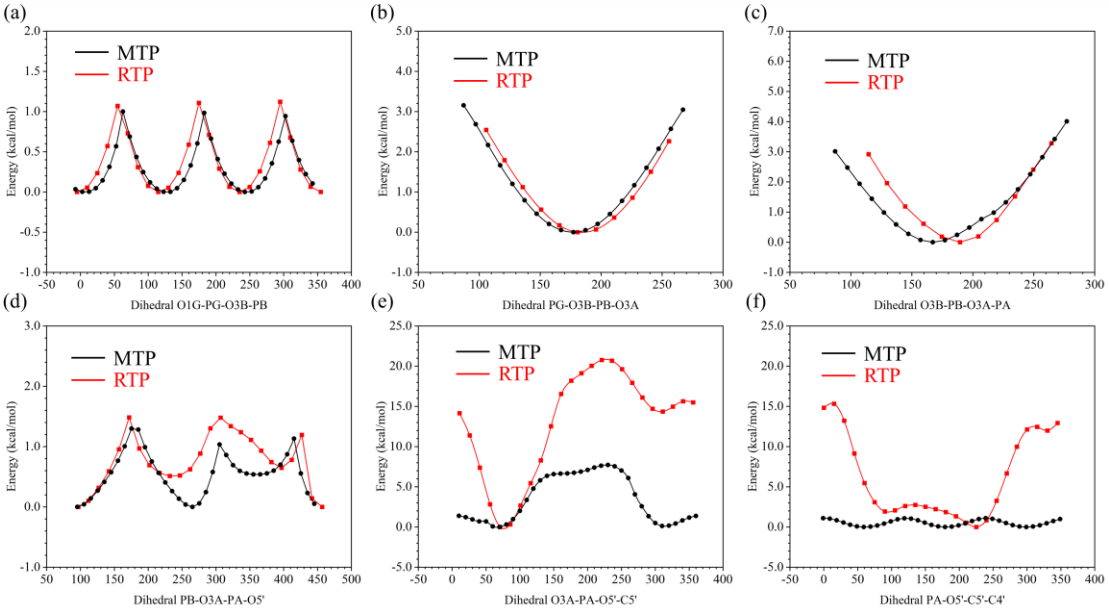

Figure 3. (a) The calculated 1D-PMF curves for the ATP-Mg^{2+} complexes transitioning from the C3 to C2 conformations using the US simulations are depicted, with bars representing standard deviations. The range of the reaction coordinate Mg^{2+}-O_α is from 1.7 to 5.9 Å, divided into 43 windows. The black curve represents the results of the MTP model, while the red and blue curves denote the outcomes obtained from the RTP models without and with the CMAP, respectively. The magnitudes of the Mg^{2+}-O_α distances and relative energies of the C3, TS, and C2 conformations are presented in parentheses. (b) The calculated 2D-CMAP using the HF/6-31+G* method is shown, with respect to the two dihedrals PB-O3A-PA-O5′ and O3B-PB-O3A-PA.

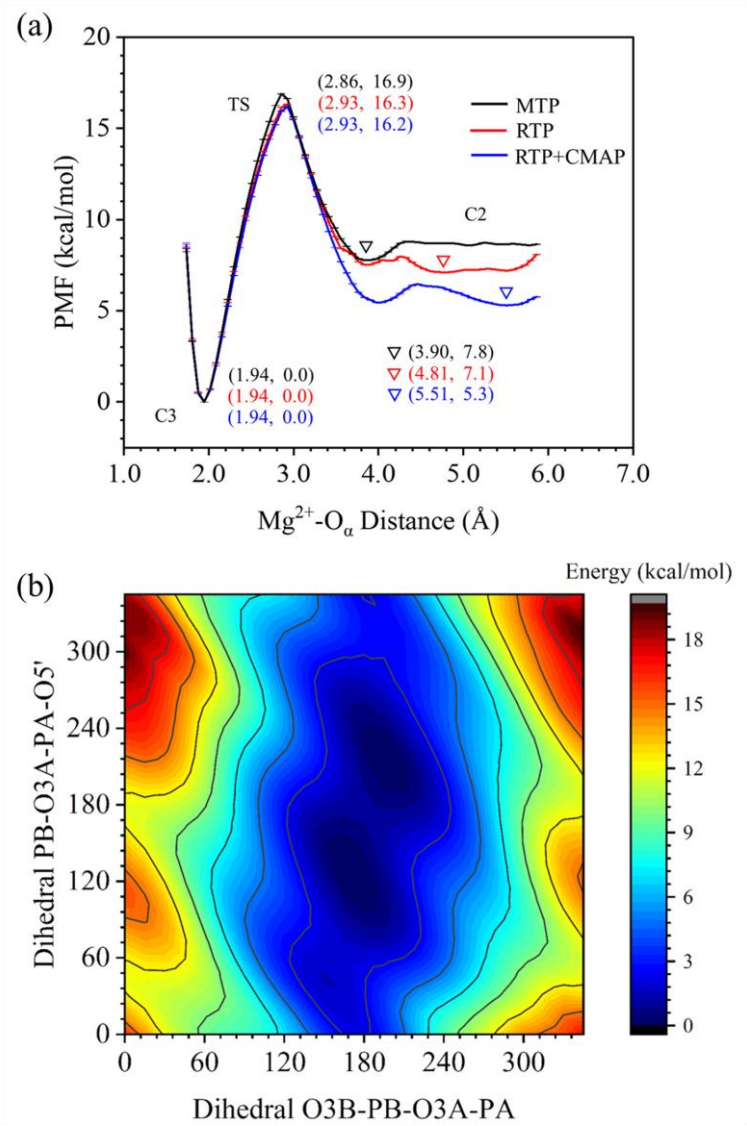

Figure 4. (a) A comparison of the QM energy $E^{QM,vdW}$ obtained from the sobEDA method and the MM energy $E^{MM,vdW}$ calculated from classical force fields. The blue dots and red triangles denote the MM vdW results calculated from the original parameters and the newly DFT-derived parameters for Mg^{2+} and ATP, respectively. The RMSD values of the blue and red MM results compared to that of $E^{QM,vdW}$ are 33.72 and 5.06 kcal/mol. (b) The calculated 1D-PMF curves for the ATP·Mg^{2+} complexes transitioning from the C3 to C2 conformations using the US simulations are depicted, with bars representing standard deviations. The black and blue curves represent the results of the RTP model with the original force fields and with the DFT-derived vdW parameters, respectively. The magnitudes of the Mg^{2+}-O_α distances and relative energies of the C3, TS, and C2 conformations are presented in parentheses.

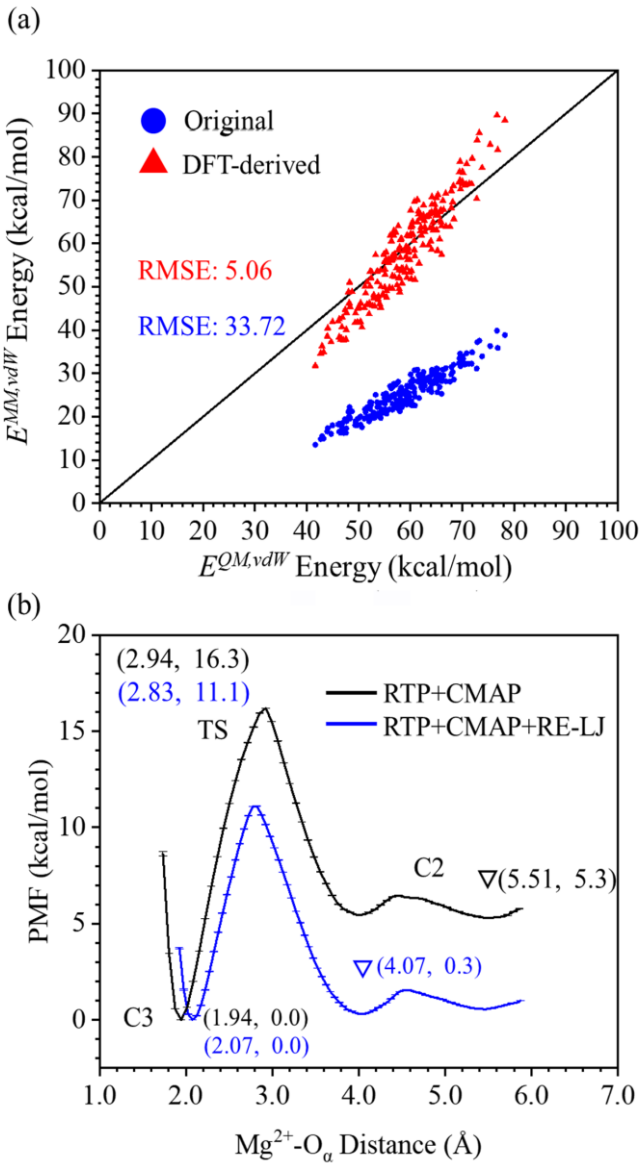

Figure 5. (a) The calculated PMF curves of ATP·Mg^{2+} transitioning from the C3 to the C2 using the US simulations. The black and blue PMF curves denote the simulation results using the original HF charges and B3LYP-derived charges in PCM model. The 2D free energy landscapes in the plots (b) and (c) show the distributions of 169 ATP structures extracted online. The simulated REMD trajectories using (b) the HF and (c) the B3LYP-derived charges were projected on the 2D free energy landscapes with respect to the PC1 and PC2 of the PCA of crystal structures.

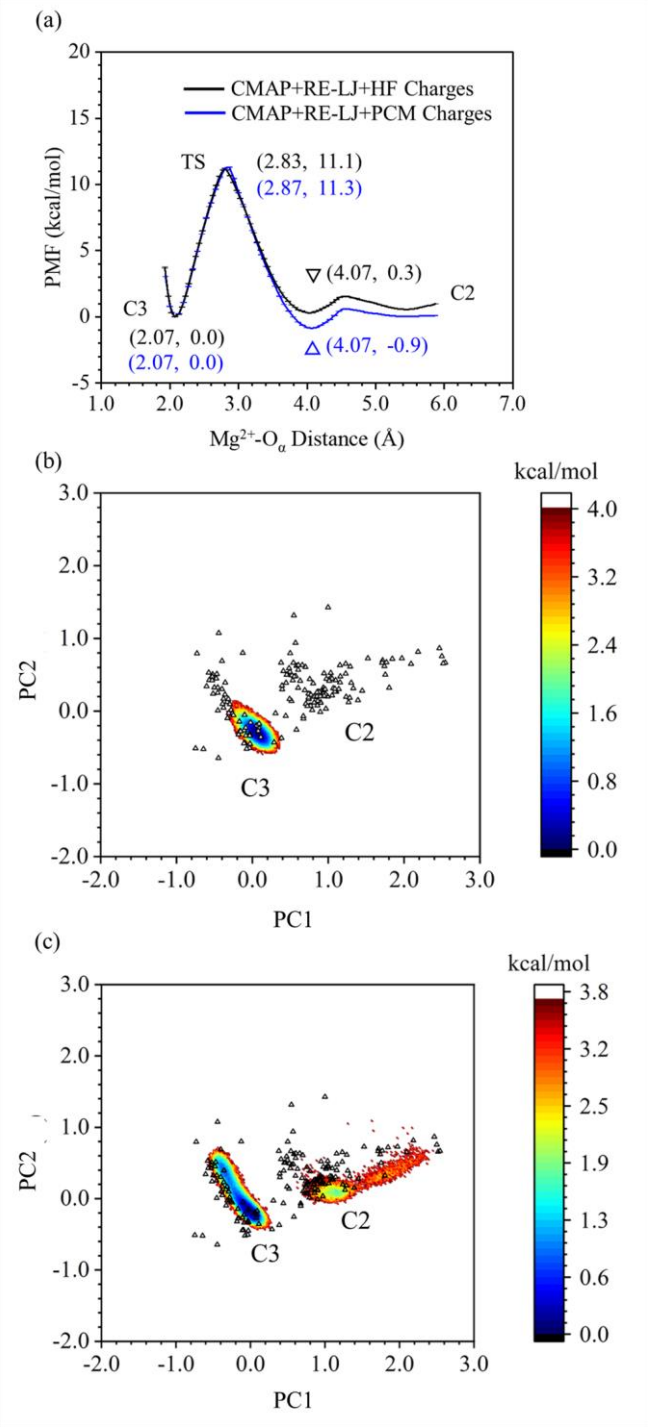

Supporting Information

Figure S1. The 1D-PMF for the conformational change from the C3 to C2 structures of the ATP·Mg^{2+} complex was estimated based on the US simulations according to the Mg^{2+}-O_α distance.

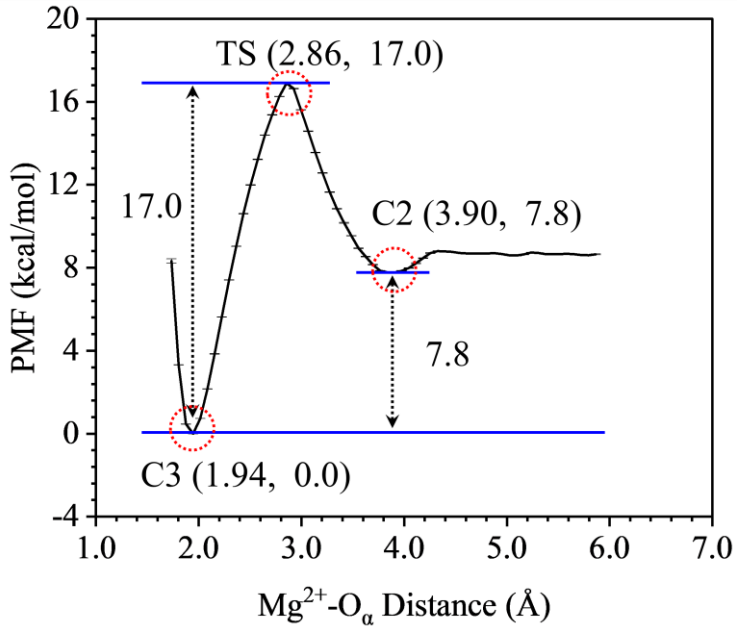

Figure S2. (a) to (f) illustrate potential energy surface scans conducted with each of the six main axes of the triphosphate moiety as rotation axes. The scans were performed using restricted optimization, with a rotation interval of 10 degrees. The red curves represent the results obtained with HF, while the black curves depict the results from MP2 calculations.

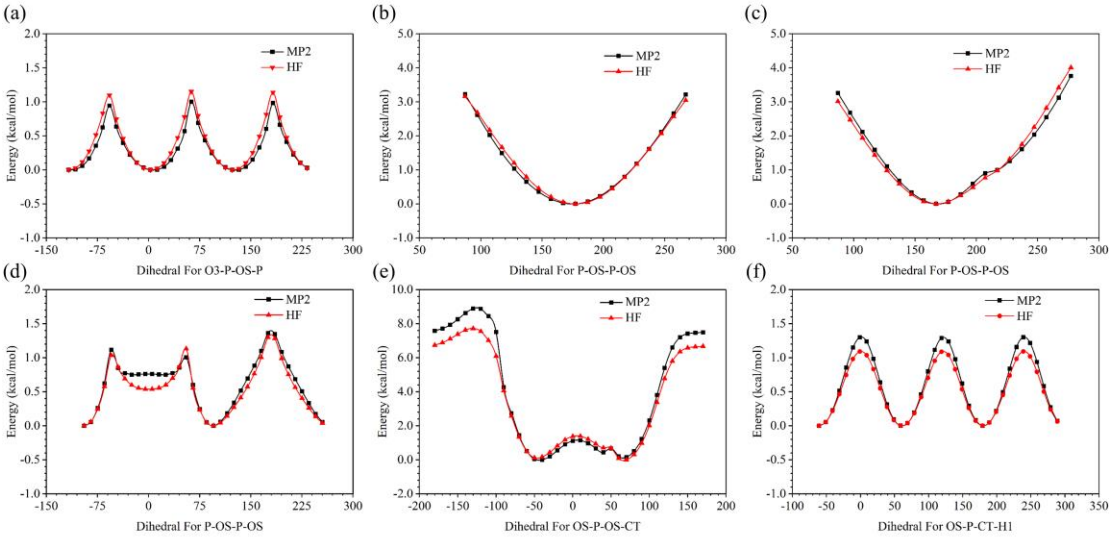

Figure S3. The calculated potential energy curves for the dihedrals O1G-PG-O3B-PB, PG-O3B-PB-O3A, O3B-PB-O3A-PA, PB-O3A-PA-O5′, O3A-PA-O5′-C5′, and PA-O5′-C5′-C4′ are shown in the plots (a) through (f), respectively. The black, red, and blue curves represent the results of the MTP model, the RTP model, and the fitted results using the *paramfit* in AMBER, respectively. The dihedral angles were scanned at 15-degree intervals using the HF/6-31+G* method. The average RMSD for the fitted data is 1.46 kcal/mol.

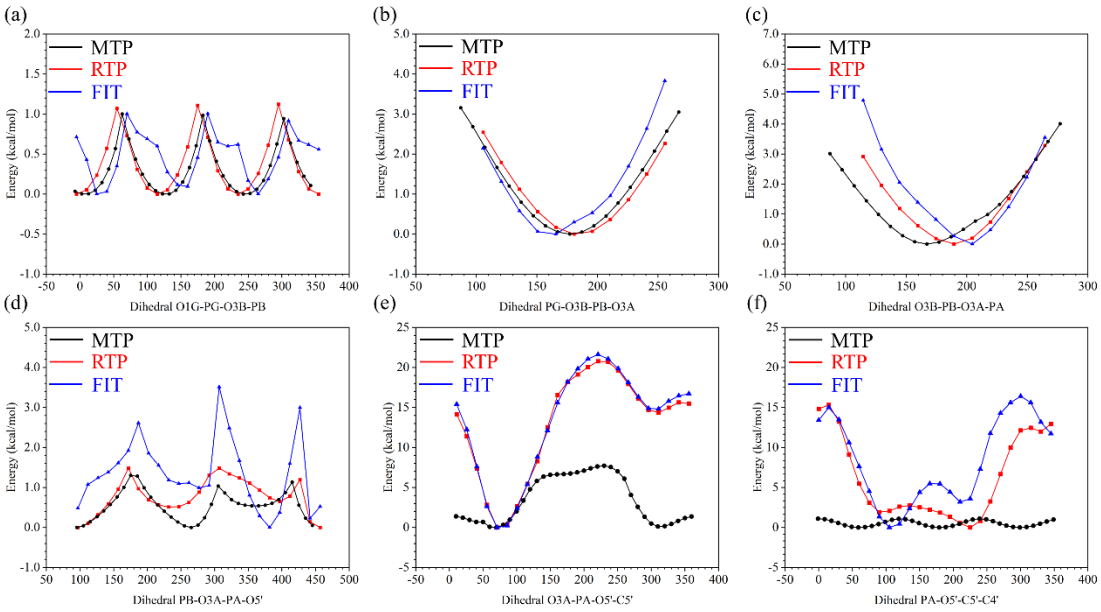

Table S1. Comparison of atomic charges obtained by RESP fitting from electrostatic potentials calculated using HF/6-31G* and B3LYP-D3(BJ)/6-311+G** in PCM.

Atom Names	HF	B3LYP-D3(BJ)	Atom Names	HF	B3LYP-D3(BJ)
O1G	-0.9526	-1.0327	C8	0.2006	0.3579
PG	1.2650	1.5524	H80	0.1553	0.1108
O2G	-0.9526	-1.0327	N7	-0.6073	-0.7078
O3G	-0.9526	-1.0327	C5	0.0515	0.0693
O3B	-0.5322	-0.6957	C6	0.7009	0.7878
PB	1.3852	1.5528	N6	-0.9019	-0.9445
O1B	-0.8894	-0.9506	H60	0.4115	0.4370
O2B	-0.8894	-0.9506	H61	0.4115	0.4370
O3A	-0.5689	-0.6819	N1	-0.7615	0.8172
PA	1.2532	1.4253	C2	0.5875	0.5309
O1A	-0.8799	-0.9041	H2	0.0473	0.0634
O2A	-0.8799	-0.9041	N3	-0.6997	-0.6838
O5*	-0.5987	-0.5669	C4	0.3053	0.4197
C5*	0.0558	-0.0142	C3*	0.2022	0.2676
H50	0.0679	0.0880	H30	0.0615	0.0867
H51	0.0679	0.0880	O3*	-0.6541	-0.7597
C4*	0.1065	0.2628	H3’	0.4376	0.4733
H40	0.1174	0.1052	C2*	0.0670	0.0740
O4*	-0.3548	-0.5296	H20	0.0972	0.1178
C1*	0.0394	0.3132	O2*	-0.6139	-0.7100
H10	0.2007	0.0994	H2’	0.4186	0.4277
N9	-0.0251	-0.2293			

Section S1: The script for using the new parameters.

1. Create a TOP file using the command "tleap -f tleap.in":

```
addatomtypes {{"O3""O""sp2"}}
addatomtypes {{"O2""O""sp2"}}
addatomtypes {{"O""O""sp2"}}
addatomtypes {{"OW""O""sp3"}}
addatomtypes {{"OY""O""sp3"}}
source leaprc.*                          # Load protein force fields you want
source leaprc.water.tip3p                # Load water models
loadAmberPrep ATP-HF/B3.prepi            # Load prepi file
loadAmberParams    ATP-HF/B3.frcmod      # Load frcmod file
……                                       # Other operations
saveamberparm name *.prmtop *.inpcrd
quit
```

2. Use "Mod.py" to modify vdW parameters and add CMAP parameters:
Please install parmed and numpy extral python packages
python mod.py -top *.prmtop -out *-out.prmtop -method B3LYP/HF